Electrochimica Acta 112 (2013) 394–402

Contents lists available at ScienceDirect

Electrochimica Acta

journal homepage: www.elsevier.com/locate/electacta

# The electrochemical performance of pitch coke anodes containing hollow carbon nanostructures and nickel nanoparticles for high-power lithium ion batteries

Canliang Ma[a,b], Yun Zhao[c], Jin Li[a,b], Yan Song[a,*], Jingli Shi[a,d,**], Quangui Guo[a], Lang Liu[a]

[a] Key Laboratory of Carbon Materials, Institute of Coal Chemistry, Chinese Academy of Sciences, Taiyuan 030001, China
[b] University of Chinese Academy of Sciences, Beijing 100049, China
[c] Institute of Molecular Science, Key Laboratory of Chemical Biology and Molecular Engineering of Education Ministry, Shanxi University, Taiyuan 030006, China
[d] School of Materials Science and Engineering, Tianjin Polytechnic University, Tianjin 300387, China

ARTICLE INFO

*Article history:*
Received 24 May 2013
Received in revised form 12 August 2013
Accepted 20 August 2013
Available online 30 August 2013

*Keywords:*
Lithium-ion battery
Pitch coke anode
Hollow carbon nanostructures
Nickel nanoparticles

ABSTRACT

Pitch cokes with abundant hollow carbon nanostructures (HCNs) and nickel nanoparticles were prepared from pitch containing nickel nanoparticles by simple heat-treatment process. The effects of nickel content and heat-treatment temperatures on the electrochemical properties were analyzed systematically. Two kinds of pitch cokes were studied in detail and both of them revealed excellent electrochemical performances, such as high reversible capacity, excellent rate capability and good cycling properties that the capacity becoming bigger with cycling. The microstructure of the samples was characterized by X-ray diffraction and transmission electron microscopy. Combined with the electrochemical performances, it was assumed that the HCNs should play an important role in the enhancing electrochemical properties as the reservoir for the lithium storage and transfer. A sample composed mainly of HCNs was fabricated to verify the hypothesis.



## 1. Introduction

Lithium ion batteries (LIB) are key components of portable equipments [1]. They are widely used as a mobile power supply for most kinds of cell phones, notebook computers, mobile devices, electric tools and electric vehicles [2]. New applications such as hybrid electric vehicles and power backup require rechargeable batteries that combine high energy density with high charge and discharge rate capability [3]. Carbon materials are used as negative electrodes for consumer LIB because they are more advantageous than other anodes in terms of cycle performance and safety. Petroleum coke was the first material used as anode for LIB [4]. It is compatible with most of electrolytes, and shows the high rate capability and good stability to the lithium repeated intercalation/de-intercalation. Moreover, a sloping discharge–charge profile instead of a low potential platform of graphite was presented, which can ensure the security of high-power lithium ion batteries (HPLIBs) [5]. However, the theoretical capacity of coke is only 186 mA h $g^{-1}$ [6], which limits its wide application. In order to take advantage of coke as anode for HPLIBs, the microstructure of coke should be modified to allow more lithium store in it [7].

Besides the lithium could insert the graphite layers, it was proved that the lithium could store in the nanopores [8–11], nanocavities [12], micropores [13,14] and other nanostructures [15,16]. Many studies demonstrated that the specific capacity and rate capability of electrodes could be enhanced effectively by increasing the porosity [8,9,12–15,17,18]. For instance, Zhou et al. [15] presented a hollow carbon cage with graphene shells obtain a high reversible capacity of 1135 mA h $g^{-1}$ at 50 mA $g^{-1}$ and an excellent charge/discharge rate of 163 mA h $g^{-1}$at 15 A $g^{-1}$. Herein, we tried to make the material with inner nanostructures which may act as the reservoir for lithium storage and transference and avoid to directly contact with electrolyte. Hollow carbon nanostructures (HCNs) like the carbon nano-onions [19] and hollow carbon cage can be prepared via a variety of processes, such as chemical reaction [19], transition-metal catalytic graphitization [15,16,20]. Therefore, the pitch containing nickel nanoparticles is a proper precursor to prepare this kind of pitch coke.

* Corresponding author. Tel.: +86 351 202 1135; fax: +86 351 202 1135.
** Corresponding author at: School of Materials Science and Engineering, Tianjin Polytechnic University, Tianjin 300387, China.
*E-mail addresses:* yansong1026@126.com (Y. Song), shijingli1963@163.com (J. Shi).

0013-4686/$ – see front matter © 2013 Elsevier Ltd. All rights reserved.
http://dx.doi.org/10.1016/j.electacta.2013.08.129

In this study, novel pitch cokes containing abundant HCNs and nickel nanoparticles were prepared by a simple thermal treatment of Ni-nanoparticle doped pitch (NNDP) [21]. According to the previous reports, these special nanostructures could provide both more lithium storage spaces [22] and better-integrated conductive network [23], which are very important to improve the performances of anode material for HPLIBs [17]. It is well known that the heat-treatment temperature affects the structure of carbon obviously, which lead to various electrochemical properties [24,25]. Meanwhile, the heat-treatment temperature will have an impact on the morphology, size and structure of nickel nanoparticle [26], resulting in the final products own different amount of HCNs and electrochemical properties. In the present work, we revealed the effects of the various Ni contents in the materials and the heat-treatment temperature on the microstructure and electrochemical performances. To explain the high performance of novel pitch cokes, we fabricated a sample made up mostly of the HCNs. To understand the present work, the contribution of carbon matrix ($C_{CM}$) and the difference value ($C_D$) between the contributions of the carbon matrix of the active anode material with the basic anode material are expressed as follows:

$$C_{CM} = \frac{C_A}{1 - \text{Ni wt.\%}} \quad (1\text{-}1)$$

$$C_D = C_{CM} - C_B \quad (1\text{-}2)$$

where $C_A$ and $C_B$ are the specific capacities of the active anode material and basic anode material, respectively.

## 2. Experimental

### 2.1. Material preparation and characterization

In this work, the NNDPs with various nickel contents were prepared according to our previous work [21]. The pitch cokes with various nickel content were heat-treated at 1000 °C for 1 h in an Argon atmosphere after a pre-oxidative treatment. These products were noted as $Ni_x$PC-1000, where "$x$" referring to the nickel content in the sample. The NNDP with nickel content of 9.44% was further heat-treated at different temperatures. The products were marked as $Ni_{9.44}$P-T, where the "T" corresponds to the heat treatment temperature. Especially, $Ni_{9.44}$P-2700 is prepared from $Ni_{9.44}$P-1000 by graphitization at 2700 °C.

To obtain the material with high HCNs content, the tetrahydrofuran soluble of pure pitch and nickel nitrate hexahydrate were used as the precursors. The sample composed mainly of HCNs was prepared by the following steps: firstly, the pure pitch is extracted with tetrahydrofuran (THF) to obtain tetrahydrofuran soluble (THFS); secondly, the nickel nitrate hexahydrate dispersed in tetrahydrofuran; after that, while stirring constantly, the THFS was mixed with the above solution and the prime product was obtained by vacuum distillation of THF. In this way, the nickel uniformly dispersed in the carbon molecules. The prime product underwent a pre-oxidative treatment and heat treatment at 1000 °C. Then, the nickel was further etched by concentrated hydrochloric acid for 7 days. Herein, the heat-treated product was named as Ni/THFSC and the final product was marked as H-Ni/THFSC.

The microstructure and morphology of the samples were characterized by X-ray Diffraction (Rigaku D/Max-RB diffractometer, using Cu $K\alpha$ radiation at 40 kV and 100 mA) and High-Resolution Transmission Electron Microscopy (HRTEM) with an energy-dispersive X-ray spectrometer (EDS) (TECNAI G2F operated at 200 kV). HRTEM samples were prepared by deposition of ground particles onto lacey carbon support films. The Ni content in the final products was determined by Inductively Coupled Plasma (ICP) analysis.

### 2.2. Electrochemical measurements

To prepare the electrodes, a mixture of active materials, acetylene black and poly (vinyl difluoride) at a weight ratio of 80:10:10 was coated onto copper foil and then dried at 120 °C under vacuum for 12 h to obtain an electrode for measurement. CR2016 coin-type cells were assembled in an argon-filled glove box (Mikrouna, China) where both moisture and oxygen levels were kept at less than 1 ppm. LiPF6 (1 mol/L) in ethylene carbonate and dimethyl carbonate (EC-DMC, 1:1, v/v) was used as the electrolyte and lithium foil was used as the counter electrode.

Electrochemical impedance spectroscopy (EIS) was measured on a CHI660 C (Huachen, Shanghai) advanced electrochemical system. An EIS was performed in the frequency range of 10 mHz–100 kHz at an amplitude of 5 mV. Galvanostatic cycling test of the assembled cells was carried out on a Land CT2001A system (Land, Wuhan) in the potential range of 0.005–3.0 V (vs. $Li^+/Li$) at different current densities at room temperature (25 ± 1 °C). For compression, the graphited mesophase carbon microbeads (G-MCMB) was tested in the same condition.

## 3. Results and discussion

### 3.1. The effect of nickel content on the electrochemical performances of $Ni_x$PC-1000

To estimate the effects of nickel content on the electrochemical properties of $Ni_x$PC-1000, the $Ni_x$PC-1000 electrodes were tested

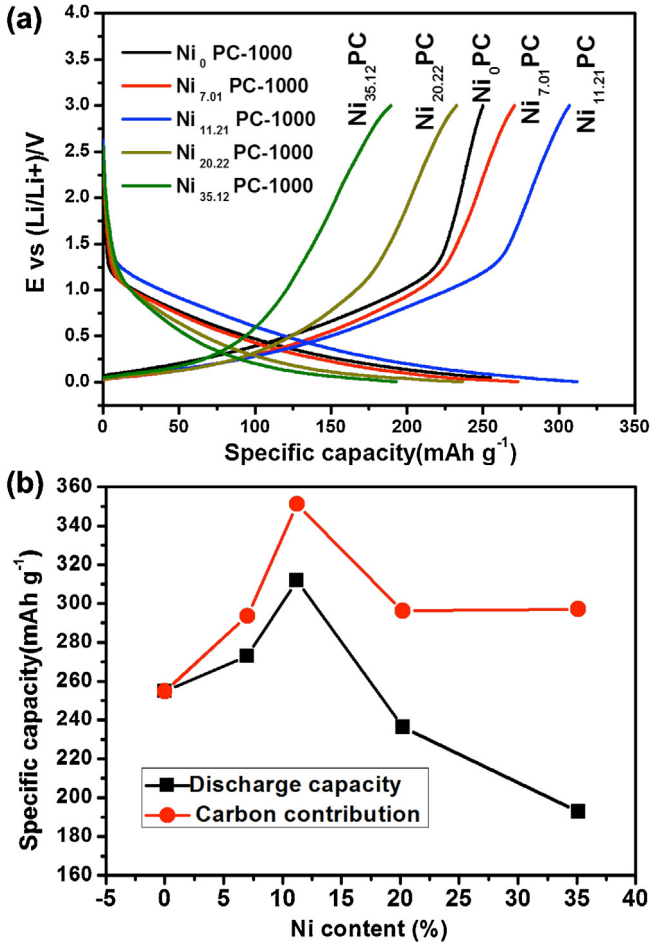


**Fig. 1.** (a) The first discharge/charge profiles of $Ni_x$PC-1000 at 100 mA $g^{-1}$. (b) Relations of discharge capacity and carbon contribution capacity with Ni contents of the $Ni_x$PC-1000.

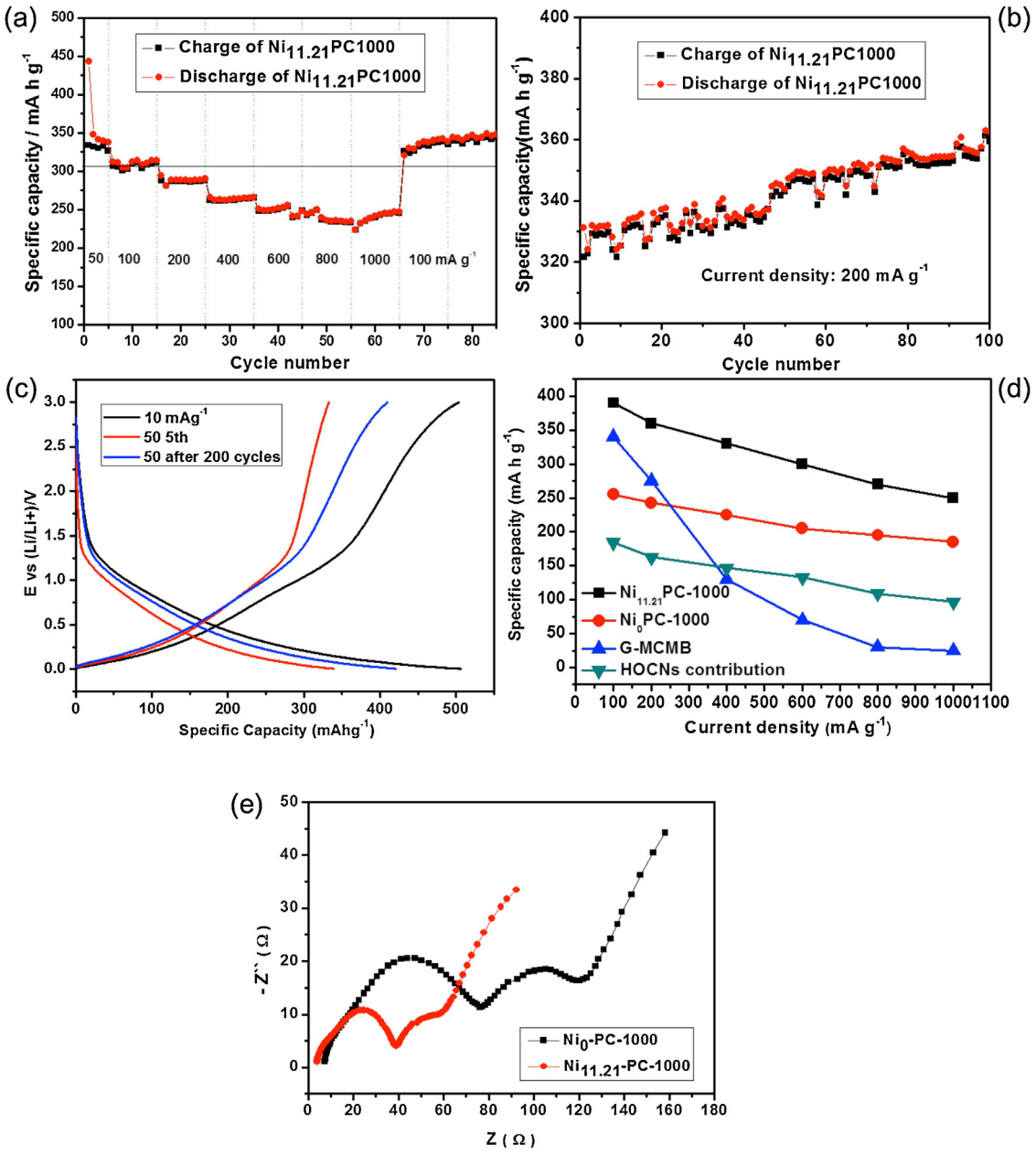


**Fig. 2.** (a) Rate and cycle performance of $Ni_{11.21}$PC-1000 for first 85 cycles. (b) Cycle performance of the $Ni_{10}$-PC at a current density of 200 mA $g^{-1}$ for the following 100 cycles. (c) Discharge/charge curves of $Ni_{11.21}$PC-1000. (d) Rate performance of $Ni_{11.21}$PC-1000, $Ni_0$PC-1000 and G-MCMB electrodes, and the contribution of nanocage like carbon. (e) Impedance spectra of $Ni_{11.21}$PC-1000 and $Ni_0$PC-1000 electrodes.

at the current density of 100 mA $g^{-1}$. The results are shown in the Fig. 1. It can be seen that they revealed the typical curves of coke electrodes [24], a little hysteresis can be seen (Fig. 1(a)). It is evident that the discharge/charge capacity increases first, and then decreases with increasing the Ni content. When the nickel percentage reached to 11.21% in the $Ni_x$PC-1000 (corresponding to $Ni_{11.21}$PC-1000), the biggest discharge/charge capacities of 311.8 and 306.8 mA h $g^{-1}$ were obtained, respectively, at the constant current density of 100 mA $g^{-1}$ for the first cycle. The discharge/charge capacities of $Ni_x$PC-1000 can be observed visually in Fig. 1(b). Taking the electrochemical inactive of nickel into consideration, the carbon matrix contribution capacities were obtained by the formula (1-1), in which the $Ni_x$PC-1000 is the active anode material. The carbon matrix contribution capacity of $Ni_{11.21}$PC-1000 reached to 351.2 mA h $g^{-1}$ at 100 mA $g^{-1}$. At the same time, it can be seen that the carbon matrix contribution capacities of $Ni_{20.22}$PC-1000 and $Ni_{35.12}$PC-1000 are lower than that of $Ni_{11.21}$PC-1000 and are as much as that of $Ni_{7.01}$PC-1000.

More electrochemical measures were tested for investigating the overall performance of $Ni_{11.21}$PC-1000, and they are shown in Fig. 2. Fig. 2(a) exhibits the rate capabilities of as-prepared $Ni_{11.21}$PC-1000. It can be seen that the capacity decreases slowly with the current density increasing from 50 to 1000 mA $g^{-1}$. The charge capacity could still reach 250 mA h $g^{-1}$ even at 1000 mA $g^{-1}$. When the current density reduced to 100 mA $g^{-1}$ again, it was found that the capacity even got larger than that at the first stage. The same behavior was also found in the following 100 cycles at 200 mA $g^{-1}$, and the charge capacity ascended to 360 mA h $g^{-1}$ (Fig. 2(b)) from 287 mA h $g^{-1}$ (Fig. 2(a)). Similarly, although the initial charge capacity was only 332.8 mA h $g^{-1}$ at 50 mA $g^{-1}$ for the

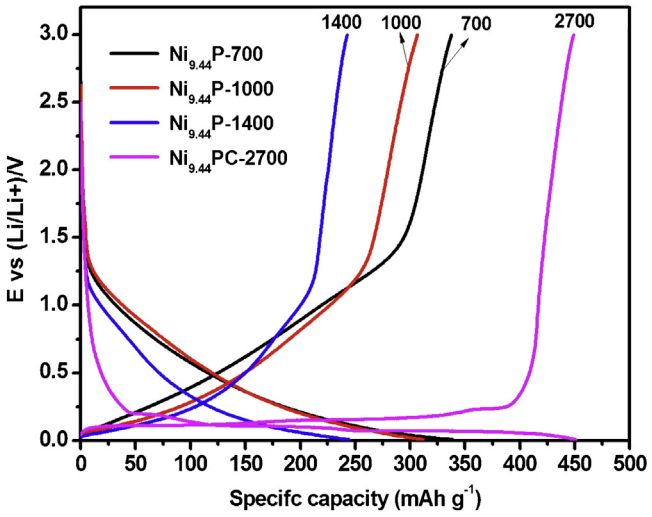


**Fig. 3.** The discharge/charge curves of $Ni_{9.44}P$-T at a current density of 100 mA $g^{-1}$.

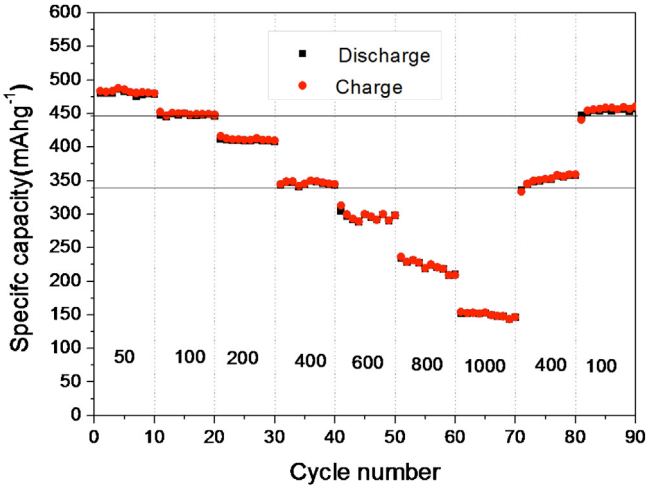


**Fig. 4.** The rate property of $Ni_{9.44}P$-2700 from 50 to 1000 mA $g^{-1}$.

fifth cycle, the charge capacity reached 410 mA h $g^{-1}$ at 50 mA $g^{-1}$ after two hundred cycles (Fig. 2(c)). Furthermore, a discharge capacity of 507 mA h $g^{-1}$ and charge capacity of 504 mA h $g^{-1}$ is obtained at 10 mA $g^{-1}$. From the discharge/charge curve, it can be found that additional capacity was discharged at 0.005–0.1 V and charged at 0.8–3.0 V, which suggest the additional Li-ions could insert into the microspaces [27] or micropores [14]. It is different from the references [14,27] that the capacity with cycling increased, neither decreased nor kept stable. The gradually increased capacity with cycling can be attributed to the structural stability of the HCNs and the activation process of the anode [10].

Fig. 2(d) shows the rate capabilities of $Ni_{11.21}$PC-1000, $Ni_0$PC-1000 and G-MCMB electrodes and the contribution of the HCNs. When taking the capacities obtained at 100 mA $g^{-1}$ as a benchmark, the retention rates of the cokes at 1000 mA $g^{-1}$ were above 60%. Due to the electrochemical inactive of nickel in the $Ni_{11.21}$PC-1000, the specific capacity difference ($C_D$) between carbon matrix of $Ni_{11.21}$PC-1000 and $Ni_0$PC-1000 was about 184 mA h $g^{-1}$ at 100 mA $g^{-1}$, according to the formula (1-1) and (1-2). The $Ni_{11.21}$PC-1000 is active anode material and the $Ni_0$PC-1000 is the basic anode material. This value decreased with the increasing current density (Fig. 2(d) blue line). These data demonstrate that there are amounts of lithium store in some carbon nanostructures, and the quantity changes with cycling and various current densities. Due to the existence of nickel nanoparticle, the electric conductivity of the electrode of $Ni_x$PC-1000 will be able obviously to enhance. After 5 cycles, impedance spectra were performed, as shown in Fig. 2(e). A semicircle, a quadrant arc and a straight line for each electrode referring to impedance for solid electrolyte interphase (SEI), charge-transfer reaction and the diffusion of lithium ion, respectively, can be obviously observed. The results indicate that the impedance of SEI and charge-transfer for $Ni_{11.21}$PC-1000 electrodes are lower than that of $Ni_0$PC-1000. The decrease of the resistance might be attributed to the improved electrical conductivity of $Ni_{11.21}$PC-1000 electrode by the embedded Ni nanoparticles.

### 3.2. The effect of heat treatment temperature on the capacity

From the above results, it can be found that the $Ni_{11.21}$PC-1000 has better electrochemical properties. Herein, the same precursor, $Ni_{9.44}P$, which means the nickel content is 9.44% in the NNDP, were heat treated at various temperatures. The products were marked as $Ni_{9.44}$P-T, where the "T" corresponds to the heat treatment temperature. Specially, the $Ni_{9.44}$P-1000 is the same sample as the $Ni_{11.21}$PC-1000 mentioned in the above part in this paper.

The discharge/charge curves of $Ni_{9.44}$P-T at a current density of 100 mA $g^{-1}$ are shown in Fig. 3. These profiles show the similar properties as the normal pitch carbon [24,27,28]. The charge capacity of $Ni_{9.44}$P-700, $Ni_{9.44}$P-1000 and $Ni_{9.44}$P-1400 reached at 339.2, 311.8 and 244.7 mA h $g^{-1}$, respectively, which could be generally explained as the porosity of pitch cokes decreased with the increasing heat-treating temperature [27]. By the same token, the potential hysteresis of $Ni_{9.44}$P-700 electrode is much higher than that of those heat treated at high temperature. The $Ni_{9.44}$P-1400 electrode shows a lower capacity because of the graphitization is not high, meanwhile, the porosity of the material is too low to provide enough spaces to store lithium ions. However, as observed that the $Ni_{9.44}$P-2700 revealed a typical discharge/charge profiles of graphitic carbon with a highest reversible capacity of 448 mA h $g^{-1}$, which is much higher than that of a graphite anode at the same condition. Besides the electrochemical inactive nickel with 11.93% in the $Ni_{9.44}$P-2700, the carbon matrix part of the anode contributed around 509 mA h $g^{-1}$ ($C_{CM}$), and it is 169 mA h $g^{-1}$ ($C_D$) larger than that of the commercial graphite. $C_{CM}$ and $C_D$ were according to the formula (1-1) and (1-2), respectively, where the $Ni_{9.44}$P-2700 is active anode material and the G-MCMB is the basic anode material. The $C_D$ also suggested that amounts of lithium stored in some other structure besides the graphite layers of $Ni_{9.44}$P-2700.

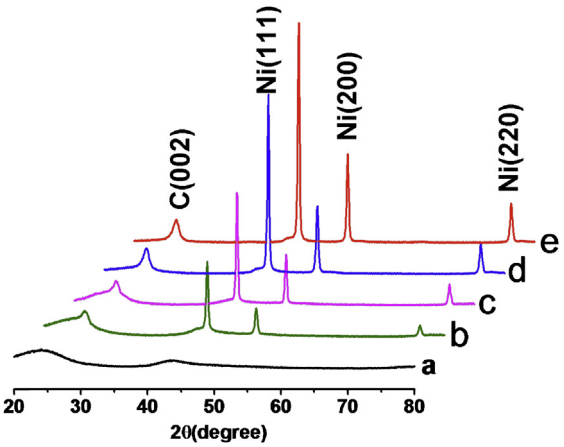


**Fig. 5.** XRD patterns of $Ni_x$PC-1000; (a) $Ni_0$PC-1000, (b) $Ni_{7.01}$PC-1000, (c) $Ni_{11.21}$PC-1000, (d) $Ni_{20.22}$PC-1000, and (e) $Ni_{35.12}$PC-1000.

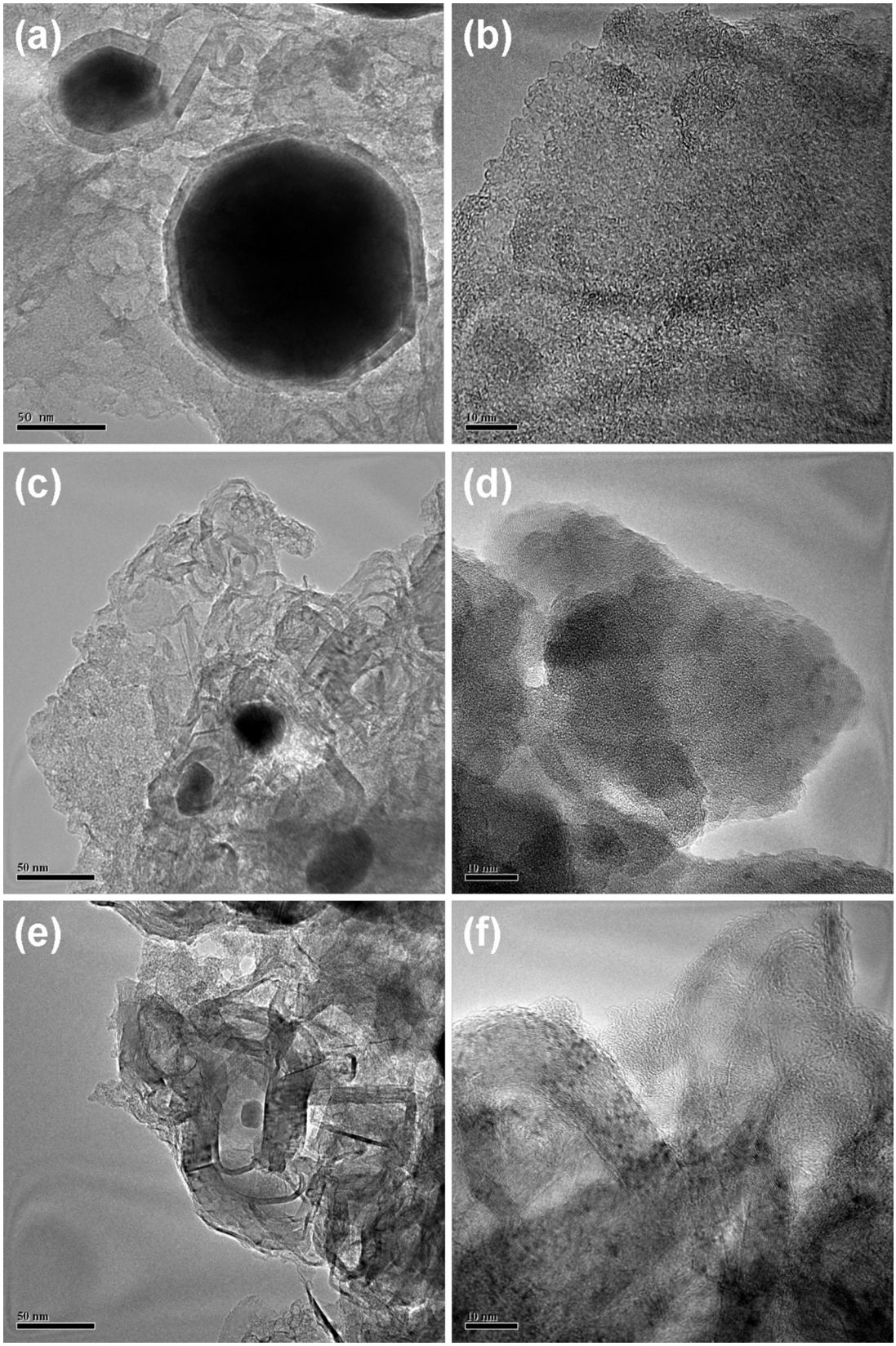


**Fig. 6.** The TEM images of $Ni_x$PC-1000: (a and b) $Ni_{11.21}$PC-1000; (c and d) $Ni_{20.22}$PC-1000; (e and f) $Ni_{35.12}$PC-1000.

Rate the performance of the $Ni_{9.44}$P-2700 electrode was evaluated (Fig. 4) too. The cell was firstly cycled at 50 mA $g^{-1}$ for ten cycles, where a stable specific capacity of around 482 mA h $g^{-1}$ was obtained. The capacity was about 350 mA h $g^{-1}$ after increasing the current density to 400 mA $g^{-1}$, which was higher than that of G-MCMB at 50 mA $g^{-1}$. Even at a high current density of 1000 mA $g^{-1}$, the specific capacity still reached to about 150 mA h $g^{-1}$. Reversible capacity of 350 and 450 mA h $g^{-1}$ at the current density of 400

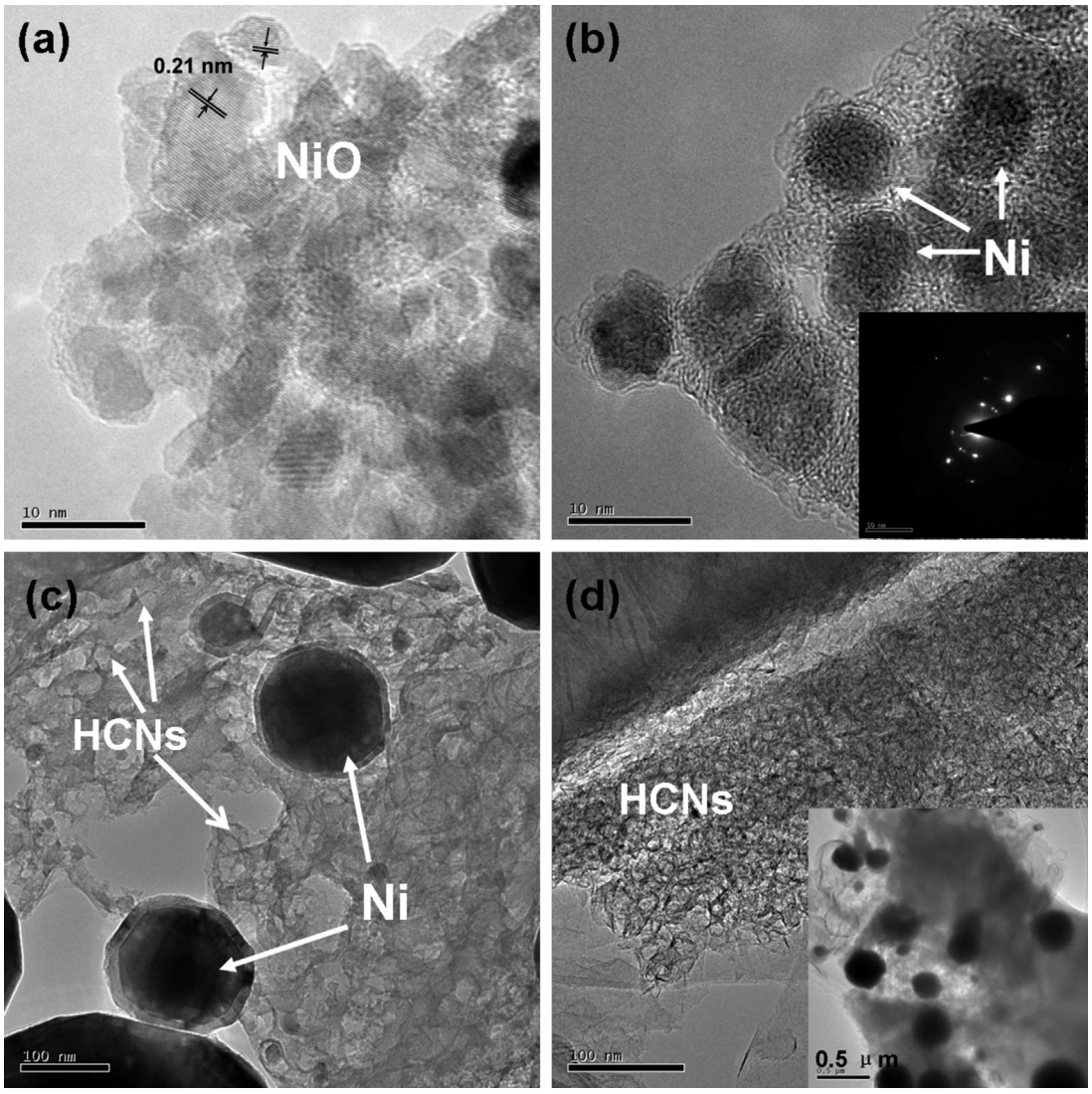


**Fig. 7.** The typical TEM images of $Ni_{9.44}P$ (a), $Ni_{9.44}P$-700 (b), $Ni_{9.44}P$-1000 (c), $Ni_{9.44}P$-2700 (d). The insert of Fig. 5(b) and (d) are the SEAD of a dark region in the (b) and other typical TEM image of $Ni_{9.44}P$-2700.

and 100 mA $g^{-1}$, respectively, were still retained after 70 cycles of charge and discharge at various current densities. These values are nearly with the capacity obtained at first cycles, indicating a good cycling stability. The results show that the kinetic characteristics of $Ni_{9.44}P$-2700 are better than G-MCMB but worse than $Ni_{11.21}PC$-1000.

### 3.3. *The explanation for high reversible capacity and good rate capability*

As mentioned above, novel pitch cokes revealed excellent electrochemical performances, such as high reversible capacity, high rate capability and good cycling properties that the capacity becoming bigger with cycling. To explain the high electrochemical performances of them, the microstructures were studied by XRD and TEM analysis.

X-ray diffraction patterns of the $Ni_xPC$-1000 are shown in Fig. 5. The diffraction peak positions observed at $2\theta = 44.51$, 51.85, and 76.37° can be assigned to the (1 1 1), (2 0 0) and (2 2 0) lattice plane of nickel (JCPDS Card No. 04-0850), respectively, suggesting the existence as the nickel in the $Ni_xPC$-1000 (patterns b–e). At the same time, it could be seen that the X-ray diffraction peak intensity of nickel is increasing with the nickel content. The broad peak ($2\theta = 26°$) is corresponding to the (0 0 2) plane of carbon, which suggests that the carbon is still amorphous although suffered a heat-treatment of 1000 °C. Meanwhile, these peaks become more and more sharp with the increasing of nickel content.

As the typical TEM images shown in the Fig. 6, one could find the HCNs exist in all the materials. They are no fixed shape with a size ranging from one to dozens of nanometers and they are all consists of several graphene layers in shells with a hollow core. The HCNs should be developed from the catalytic graphitization of nickel nanoparticle and transference of nickel [20]. Fortunately, intermediate processes were found and shown in the Fig. 6(a). The graphitic carbon shells with big nickel particle as core and the graphitic carbon hollow shells are clearly observed, indicating the small nickel nanoparticles could escape from the original position and left the hollow shell to form the HCNs. The same intermediate processes were also found in the $Ni_{20.22}PC$-1000 (Fig. 6(c)) and $Ni_{35.12}PC$-1000 (Fig. 6(e)). On the other hand, there was no small nickel nanoparticles existing in the amorphous carbon matrix of $Ni_{11.21}PC$-1000 as shown in Fig. 6(b). Different from the $Ni_{11.21}PC$-1000, there are lots of nickel nanoparticle (dark points in Fig. 6(c) and (d)) evenly dispersed in the amorphous carbon region. What

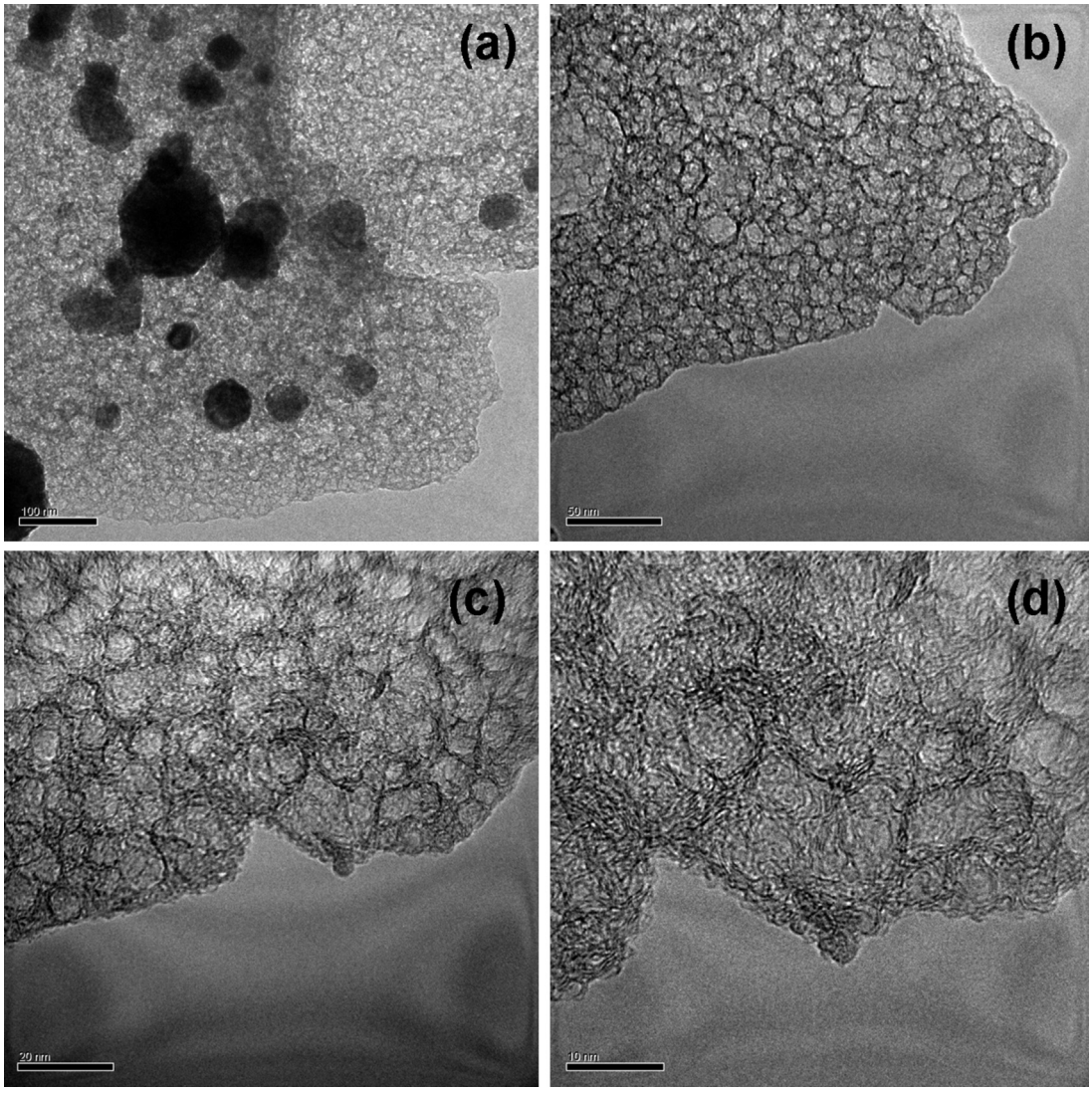


**Fig. 8.** The TEM images of Ni/THFSC (a) and HCNs (b–d), respectively.

is more, $Ni_{35.12}$PC-1000 has a larger amount of nickel nanoparticle than $Ni_{11.21}$PC-1000, abundant nickel nanparicles with several nanometers dispersed in the whole material (Fig. 6(f)). It seems that the nickel nanoparticles might do not completely take part in the processes of forming the HCNs, which means that the nickel nanoparticles in the $Ni_{20.22}$PC-1000 and $Ni_{35.12}$PC-1000 may be excess in this system. It may explain why the reversible capacities of $Ni_{20.22}$PC-1000 and $Ni_{35.12}$PC-1000 are much less than that of $Ni_{11.21}$PC-1000.

At the same time, the TEM images of $Ni_{9.44}$P-T were also taken to study the microstructure and shown in the Fig. 7. The data of inter-layer spacing can be indexed into the nickel oxide with several nanometers and evenly disperses in the pitch matrix. After the heat-treatment at 700 °C for 1 h, the nickel oxide was reduced to nickel by carbon and the nickel nanoparticle fused to nanosphere with the size range from 5 to 10 nm (Fig. 7(b)). The corresponding SAED pattern was shown in the inset of Fig. 7(b). Meanwhile, they were forming the carbon shells. Under this temperature, the nickel nanoparticles were tightly wrapped by carbon shell in the amorphous carbon matrix. When the temperature rises to 1000 °C it could be observed from the Fig. 7(c) that the microstructure had changed obviously. There are amount of the HCNs with various sizes, onion like carbon nanostructures with the nickel as core and the intermediate phase between them. Fig. 7(d) shows the representative TEM image of $Ni_{9.44}$-2700. There is still lots of nickel nanoparticle in the material (insert of Fig. 7(d)).

From the above-mentioned electrochemical and microstructure analysis, one could observe that these pitch cokes have three main nanostructure of carbon, nickel nanoparticle and HCNs. Besides the carbon, the reversible capacity of anode material should be related to the HCNs because the nickel is electrochemical inactive. Considering the limits of graphite layers on storing lithium and the kinds of mechanism for the storage of lithium in carbon, it is supposed that the excess lithium might be stored in the HCNs. Consequently, the amount of lithium storing in the HCNs should be as same as the difference value ($C_D$) between the contribution of carbon matrix of the active anode material ($C_{CM}$) with the basic anode material ($C_B$). The HCNs and nickel nanoparticles enhanced the electrochemical performances.

For this reason, it could be explained that the excessive capacity of $Ni_x$PC-1000 than that of $Ni_0$PC-1000 is attributed to the excessive lithium storing in the HCNs. Thus, it also might explain why the reversible capacity of carbon contribution of $Ni_{20.22}$PC-1000 and $Ni_{35.12}$PC-1000 is lower than that of $Ni_{11.21}$PC-1000. There were amounts of nickel nanoparticles disappeared in the carbon matrix of $Ni_{20.22}$PC-1000 and $Ni_{35.12}$PC-1000 did not play a role in

forming the HCNs. So the amount of HCNs in the $Ni_{20.22}$PC-1000 and $Ni_{35.12}$PC-1000 might be much smaller than that of $Ni_{11.21}$PC-1000, which led to the low reversible capacity of carbon contributed part. As a logical consequence of this special nanostructure, the rate capability and cycling performance of $Ni_{11.21}$PC-1000 and $Ni_{9.44}$P-2700 enhanced obviously.

According to above speculation, the Ni/THFSC was prepared, in which the Ni content is 43.20% analyzed by ICP. The microstructure and electrochemical properties of these two samples were studied and shown in Figs. 8 and 9.

As shown in Fig. 8(a), the Ni/THFSC has the similar nanostructure to the $Ni_x$PC-T, which has three kinds of structure including carbon matrix, nickel nanoparticle and the HCNs. Due to the carbon precursor is the THFS and the nickel precursor is the nickel nitrate hexahydrate, both precursors dispersed in the THF and they could achieve molecule-level dispersion. As a result, although the Ni/THFSC has high nickel content, it did not find the large number of nickel nano particles disperse in the carbon matrix which is different from the $Ni_{20.22}$PC-1000 and $Ni_{35.12}$PC-1000. Therefore, most of the nickel nanoparticles should play the role in forming the HCNs. At the same time, it could be observed from Fig. 8(b–d) that the HCNs in both Ni/THFSC and H-Ni/THFSC are uniform with an average diameter of 10 nm. This kind of nanostructure could play an important role in storing lithium according to the mechanism of lithium stored in low temperature carbon [14].

The rate performance of the Ni/THFSC and H-Ni/THFSC electrodes were tested (Fig. 9(a)) too. The cells were firstly cycled at 100 mA $g^{-1}$ for ten cycles, where the stable specific capacity of around 240 and 361 mA h $g^{-1}$, respectively, were obtained for Ni/THFSC and H-Ni/THFSC, respectively. When the current density increased to 200 mA $g^{-1}$, the reversible capacity of H-Ni/THFSC still reached 315 mA h $g^{-1}$. It is interesting that the reversible specific capacity of both kinds of anodes did not decrease obviously when the current density increased from 400 to 1000 mA $g^{-1}$. In detail, for the H-Ni/THFSC, the charge capacity of 283.8, 273.9, 256.9 and 251.7 mA h $g^{-1}$ were still obtained at the current density of 400, 600, 800 and 1000 mA $g^{-1}$, respectively (Fig. 9(b)). When it comes to the Ni/THFSC, the values of 194.9, 181, 171.6 and 168 mA h $g^{-1}$ were obtained at the current density of 400, 600, 800 and 1000 mA $g^{-1}$, respectively (Fig. 9(b)). These rate properties are higher than any other else mentioned anodes in this present work.

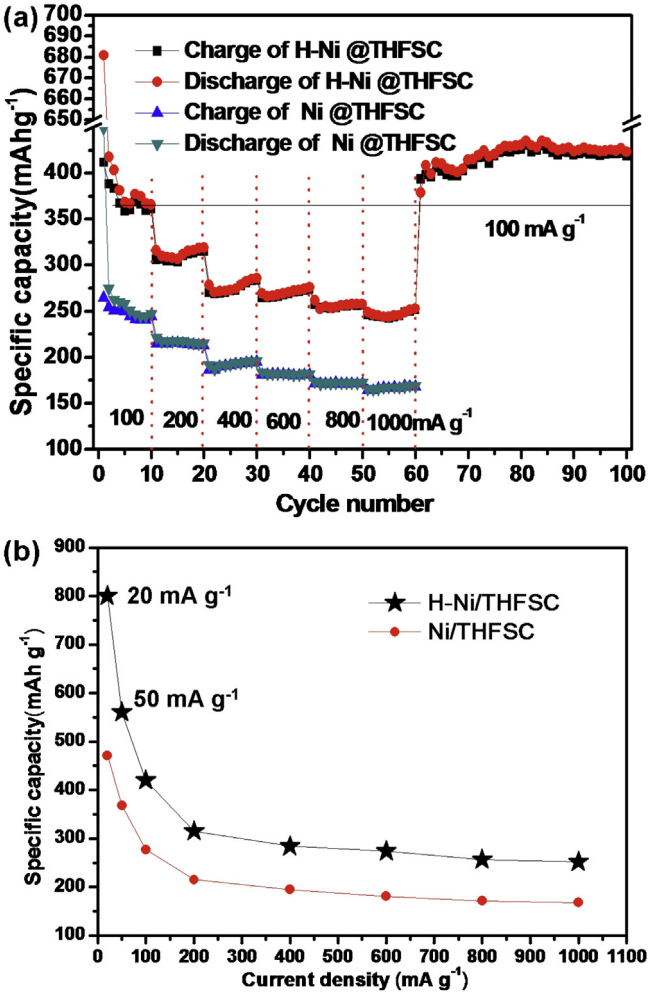


**Fig. 9.** The rate performance of Ni/THFSC and H-Ni/THFSC at the current density from 20 to 1000 mA $g^{-1}$.

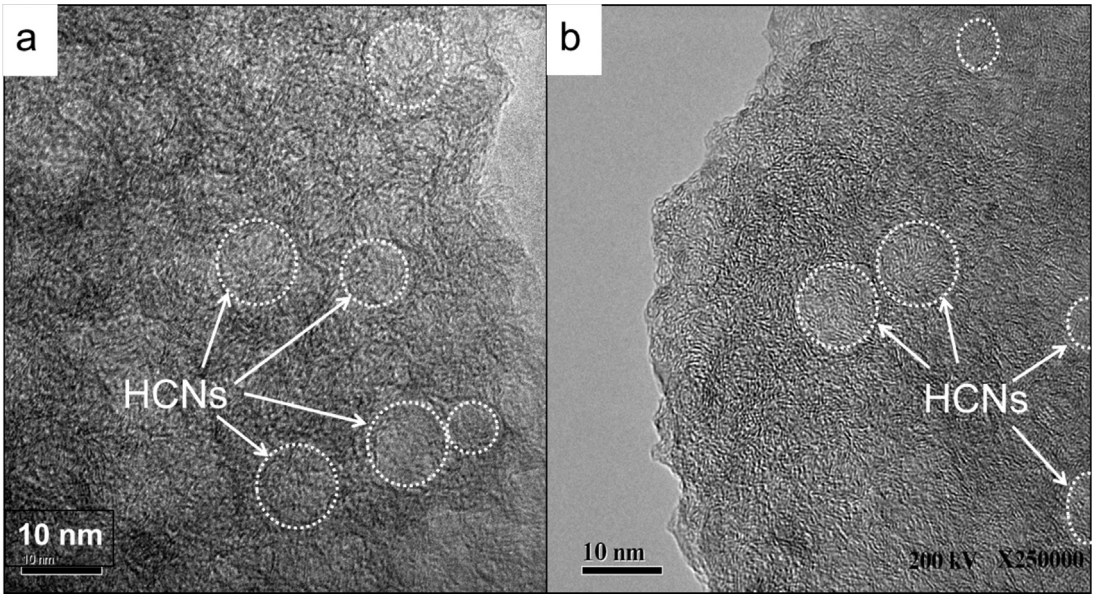


**Fig. 10.** The HRTEM images of HCNs in H-Ni/THFSC before (a) and after (b) the battery test.

When the current density decreased to 100 mA $g^{-1}$, it could be found that the discharge/charge capacities of H-Ni/THFSC anode was increasing and stabilized at 420 mA h $g^{-1}$, indicating a good cycling performance, which is similar to the $Ni_{11.21}$PC-1000. As shown in Fig. 9(b), when the current density reduced to the 50 and 20 mA $g^{-1}$, the higher reversible capacity of 560 and 800 mA h $g^{-1}$, respectively, were obtained. It should be attributed to their high content of HCNs. In consideration of the limited amount of lithium insert the graphite layers of carbon matrix, large number of lithium store in the HCNs. And these results also proved that HCNs act as the reservoir for the lithium storage and transfer [10]. Vast lithium in the forming of lithium molecules ($Li_x$, $x \geq 2$) or lithium clusters could store in the HCNs at small current density. It is worth noting that the reversible capacities of H-Ni/THFSC obtained at different current densities are about that of $Ni_{11.21}$PC-1000. Considering the quantity of carbon of $Ni_{11.21}$PC-1000 is much higher than that of H-Ni/THFSC, the HCNs of H-Ni/THFSC store more lithium ions. This phenomenon also verifies the hypothesis.

The micro structural change before and after the battery test was examined and shown in Fig. 10. The HRTEM images of HCNs in H-Ni/THFSC before and after the battery test demonstrate that there are no apparent changes of HCNs in the morphology, size and structure. What is more, the texture of the carbon matrix after the battery test becomes much clearer than that of the initial carbon matrix. It should be due to repeated discharge/charge processes leading to more microspaces for lithium ion storage, which give evidence that the capacity became bigger with cycling. Thus, the microstructure is stable, meanwhile, the stable cycle performance and excellent rate property also back up this view.

According to the above results and analyses, it could be found that nickel nanoparticles catalyzed the carbon around them to form the HCNs, and then they escaped from these carbon shell to grow into the bigger Ni particles or further catalyzed other carbon to produce more HCNs in these pitch cokes. Combined the microstructure with the electrochemical performances, it was assumed that the HCNs should play an important role in the enhancing electrochemical properties, such as reversible capacity, rate capability and cycling stability. The HCNs act as the reservoir for the lithium storage and transfer. At the same time, the introduction of nickel nanoparticles into the coke system enhanced the electrical conductivity, which was in favor of the improvement of rate capability. By comparing of H-Ni/THFSC with Ni/THFSC, HCNs plays a more important role in improving the electrochemical performance of carbon electrode.

## 4. Conclusions

In conclusion, we demonstrated that abundant HCNs and nickel nanoparticles can be effectively introduced into pitch coke by a simple heat-treatment of NNDP. The introduction of these HCNs in pitch cokes is favorable to enhance the electrochemical properties in terms of the reversible capacity, cycle performance and rate capability of pitch coke. This low-cost pitch cokes are very promising anode materials with good practicability for HPLIB.

## Acknowledgements

This work was financially supported by the National Basic Research Program of China (973 Program, No. 2011CB605802), Natural Science Foundation of Shanxi Province (No. 2012011219-3) and the Outstanding Young Talent Fund of Shanxi Institute of Coal Chemistry, Chinese Academy of Sciences.

## References

[1] N. Singh, C. Galande, A. Miranda, A. Mathkar, W. Gao, A.L.M. Reddy, A. Vlad, P.M. Ajayan, Paintable battery, Sci. Rep. UK 2 (2012) 1.
[2] M. Armand, J.M. Tarascon, Building better batteries, Nature 451 (2008) 652.
[3] K. Kang, Electrodes with high power and high capacity for rechargeable lithium batteries, Science 311 (2006) 977.
[4] T. Nagaura, K. Tozawa, Lithium ion rechargeable battery, Prog. Batteries Solar Cells 9 (1990) 209.
[5] H. Shi, Coke vs. graphite as anodes for lithium-ion batteries, J. Power Sources 75 (1998) 64.
[6] Y. Kida, K. Yanagida, A. Funahashi, T. Nohma, I. Yonezu, Electrochemical characteristics of graphite, coke and graphite coke hybrid carbon as negative electrode materials for lithium secondary batteries, J. Power Sources 94 (2001) 74.
[7] X. Zhou, L. Ma, J. Yang, B. Huang, Y. Zou, J. Tang, J. Xie, S. Wang, G. Chen, Properties of graphitized boron-doped coal-based coke powders as anode for lithium-ion batteries, J. Electroanal. Chem. 698 (2013) 39.
[8] E. Buiel, J.R. Dahn, Li-insertion in hard carbon anode materials for Li-ion batteries, Electrochim. Acta 45 (1999) 121.
[9] Q. Wang, H. Li, L.Q. Chen, X.J. Huang, Monodispersed hard carbon spherules with uniform nanopores, Carbon 39 (2001) 2211.
[10] L. Qie, W.M. Chen, Z.H. Wang, Q.G. Shao, X. Li, L.X. Yuan, X.L. Hu, W.X. Zhang, Y.H. Huang, Nitrogen-doped porous carbon nanofiber webs as anodes for lithium ion batteries with a super high capacity and rate capability, Adv. Mater. 24 (2012) 2047.
[11] N.A. Kaskhedikar, J. Maier, Lithium storage in carbon nanostructures, Adv. Mater. 21 (2009) 2664.
[12] K. Tokumitsu, H. Fujimoto, A. Mabuch, T. Kasuh, High capacity carbon anode for Li-ion battery: a theoretical explanation, Carbon 37 (1999) 1599.
[13] J. Hu, H.L. Li, X.J. Huang, Influence of micropore structure on Li-storage capacity in hard carbon spherules, Solid State Ionics 176 (2005) 1151.
[14] Y.P. Wu, C.R. Wan, C.Y. Jiang, S.B. Fang, Y.Y. Jiang, Mechanism of lithium storage in low temperature carbon, Carbon 37 (1999) 1901.
[15] G.M. Zhou, D.W. Wang, X.Y. Shan, N. Li, F. Li, H.M. Cheng, Hollow carbon cage with nanocapsules of graphitic shell/nickel core as an anode material for high rate lithium ion batteries, J. Mater. Chem. 22 (2012) 11252.
[16] C.L. Ma, Y. Zhao, J. Li, Y. Song, J. Shi, Q.G. Guo, L. Liu, Synthesis and electrochemical properties of artificial graphite as an anode for high-performance lithium-ion batteries, Carbon (2013), http://dx.doi.org/10.1016/j.carbon.2013.07.089.
[17] S.B. Yang, H.H. Song, X.H. Chen, Electrochemical performance of expanded mesocarbon microbeads as anode material for lithium-ion batteries, Electrochem. Commun. 8 (2006) 137.
[18] L.F. Shen, X.G. Zhang, E. Uchaker, C.Z. Yuan, G.Z. Cao, $Li_4Ti_5O_{12}$ nanoparticles embedded in a mesoporous carbon matrix as a superior anode material for high rate lithium ion batteries, Adv. Energy Mater. 2 (2012) 691.
[19] F.D. Han, B. Yao, Y.J. Bai, Preparation of carbon nano-onions and their application as anode materials for rechargeable lithium-ion batteries, J. Phys. Chem. C 115 (2011) 8923.
[20] W. Lian, H. Song, X. Chen, L. Li, J. Huo, M. Zhao, G. Wang, The transformation of acetylene black into onion-like hollow carbon nanoparticles at 1000 °C using an iron catalyst, Carbon 46 (2008) 525.
[21] J. Li, Q.G. Guo, J.L. Shi, X.Q. Gao, Z.H. Feng, Z. Fan, L. Liu, Preparation of Ni nanoparticle-doped carbon fibers, Carbon 50 (2012) 2045.
[22] I. Mochida, C.H. Ku, Y. Korai, Anodic performance and insertion mechanism of hard carbons prepared from synthetic isotropic pitches, Carbon 39 (2001) 399.
[23] J.C. Yue, X.Y. Zhao, D.G. Xia, Electrochemical lithium storage of C/Co composite as an anode material for lithium ion batteries, Electrochem. Commun. 18 (2012) 44.
[24] A. Mabuchi, K. Tokumitsu, H. Fujimoto, T. Kasuh, Charge discharge characteristics of the mesocarbon miocrobeads heat treated at different temperatures, J. Electrochem. Soc. 142 (1995) 1041.
[25] H. Fujimoto, Development of efficient carbon anode material for a high-power and long-life lithium ion battery, J. Power Sources 195 (2010) 5019.
[26] M. Salavati-Niasari, F. Davar, Z. Fereshteh, Synthesis of nickel and nickel oxide nanoparticles via heat-treatment of simple octanoate precursor, J. Alloys Compd. 494 (2010) 410.
[27] I. Mochida, C.H. Ku, S.H. Yoon, Y. Korai, Anodic performance and mechanism of mesophase-pitch-derived carbons in lithium ion batteries, J. Power Sources 75 (1998) 214.
[28] J.R. Dahn, T. Zheng, Y.H. Liu, J.S. Xue, Mechanisms for lithium insertion in carbonaceous materials, Science 270 (1995) 590.